Modelling of damage in historical masonry façades subjected to a combination of ground settlement and vibrations

Paul A. Korswagen*[1], Michele Longo[1], Alfonso Prosperi[1], Jan G. Rots[1]
and Karel C. Terwel[1]
[1] Delft University of Technology, Stevinweg 1, 2628 CN Delft, The Netherlands
P.A.KorswagenEguren@tudelft.nl

Abstract. Historical masonry façades are sensitive to various damaging processes. A recent study, looking at the initiation and progression of cracks in masonry, in the range of 0.1 to 5 mm in width and thus corresponding to light damage [1], has allowed for the calibration of finite-element models that include a material model capable of accurately replicating this damage and which is populated with material properties corresponding to existing structures [6]. The models, which also include a soil-structure interaction boundary designed to account for the effect of the soil during earthquake vibrations [7], have been used to determine the fragility of masonry buildings via the proxy of 2D walls [2]. In the study presented herein, the finite element models are employed to replicate the geometry of (historical) masonry facades to determine their sensitivity to light damage as a consequence of the two damaging processes observed to be most common for this type of façade, namely (differential) settlements and (earthquake) vibrations [3].

The masonry façades were first pre-damaged via settlement distortions which generate just-visible cracks in the order of 0.1 mm to 1 mm in width. Then, an acceleration time history corresponding to two different Dutch earthquake events and two recordings of traffic-induced building vibrations [9] were separately applied at the base of the models. In this manner, the effect of existing damage could be assessed in regards to the aggravation generated by vibrations. The settlement part of the study revealed that long façades were more vulnerable to applied soil distortions, for instance. Then, subsequent vibrations further increased damage for intensities measured with a peak ground velocity (PGV) larger than 2 mm/s while the control set of virgin or uncracked façades remained undamaged at this PGV. At 32 mm/s, many pre-damaged façades also exceeded the light damage range. At equal PGV, the traffic vibrations, with a larger number of effective cycles, resulted in increased damage aggravation in comparison to the earthquake recordings.

Keywords: Masonry Modelling, Settlements, Vibrations, Damage Aggravation

1 Introduction

Masonry structures are ubiquitous in the Netherlands; from elegant water towers to historical façades along city canals, masonry dominated the landscape and is still employed in most housing today in load bearing walls or outer veneers. Similarly, the Netherlands is rich in clayey and peaty soft soils; the land is flat and the water table is high, close to the surface. While traditional windmills, quay walls, and other infrastructure pioneered timber (and later concrete) piled foundations, housing did not transition away from shallow strip foundations until 1925, if clayey or peaty soil was present, and was still used into the late 1970s for sandy soils. Consequently, many historical masonry structures today, rest on shallow strip foundations supported by soft soils. Changes in the water table, new constructions, and more extreme seasonal variations in precipitation, in conjunction with heterogenous soil profiles, for example, have led to extended settlement-induced damage throughout the country [3, 17, 18].

Furthermore, the heavily industrialized Netherlands is riddled with roads and railroads, large (housing) developments, major construction activities, and many small gas fields. In particular, the case of the Groningen gas field, in the north of the country, has led to perceivable induced seismicity and subsidence. These various phenomena cause vibrations that can also affect buildings.

1.1 Objective

In this light, investigating the effect of vibrations on masonry façades already subjected to settlement deformations has become a paramount endeavour when attempting to understand crack-based damage visible in many historical buildings [3]. In this brief paper, we aim to examine a few non-linear models of historical masonry façades, pre-damaged by applied settlement distortions, and further damaged by small vibrations characteristic of induced earthquakes and road traffic. Our goal is to quantify the effect of the existing damage and to determine when this damage is expected to be aggravated, also observing the effect of other parameters such as the length of the façade and their material strength.

2 Methodology

2.1 Background studies

For the purpose of studying the effect of existing damage on historical masonry façades when subjected to vibrations, we make use a previously-calibrated modelling strategy that includes a non-linear material model for masonry, an experimental campaign with masonry walls surveyed at the crack initiation and propagation stages, an extrapolation study on walls and earthquake vibrations, a desk study on the type of settlement damage typically observed with measurements of bed-joint deformations, and modelling investigations of façades subjected to ground distortions. These earlier studies and their relationship to the focus of this paper is illustrated in the flowchart of Figure 1 and a small description of each stage is collected next.

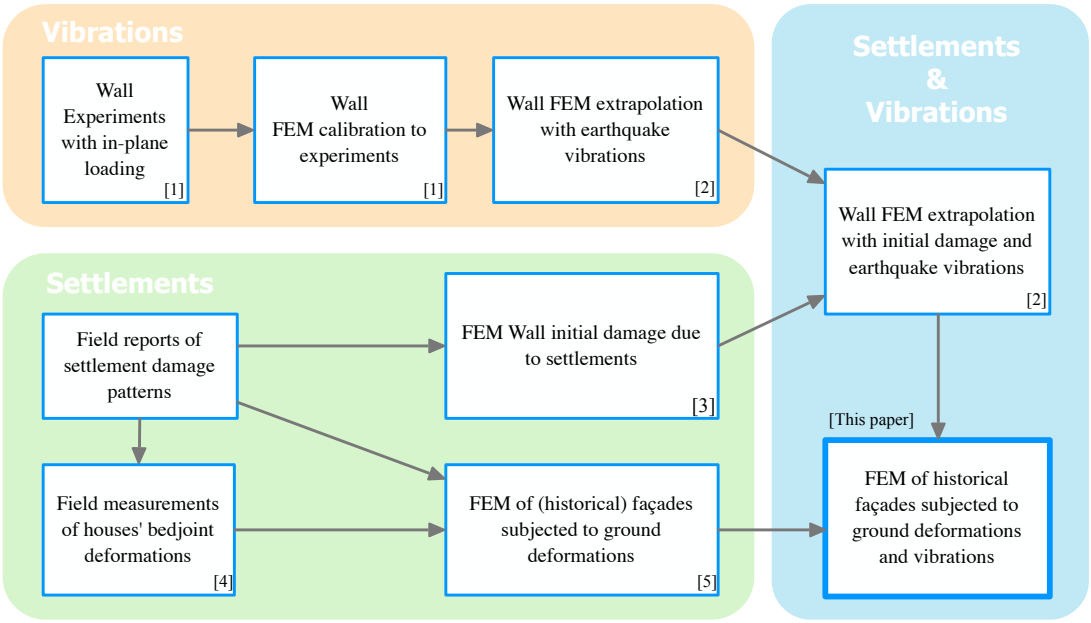

Fig. 1. Flowchart of earlier studies leading to the focus of this paper. Brackets refer to earlier studies.

Wall experiments. Several full-scale walls with or without openings for a window were tested in-plane with a one- or two-way cyclic, imposed horizontal drift [1]. Using Digital Image Correlation, the initiation of cracks, at a width of 0.1mm, and their progression throughout the repeated loading, was monitored and quantified. The walls were built of fired-clay bricks in a single-wythe stretcher bond with a cement-lime-based mortar. Additional characterisation tests, like bond-wrench of compression wallet tests were used to obtain elastic, strength, and toughness properties of the masonry. Earlier characterisation tests on actual building samples were used to formulate the characteristics of the replicated masonry [6].

Wall calibration models. Based on the experiments, FEM models were calibrated in terms of stiffness, strength, hysteresis and crack patterns. The Engineering Masonry Model [14], a material model developed to include the orthotropy of masonry, with linear tension softening, secant loading/unloading for compression, and elastic unloading for shear, was employed and the input properties were further refined to replicate the behaviour of the experiments.

Wall extrapolation models. The calibrated wall models were modified as little as possible to include a realistic boundary condition, in contrast to the top steel beam of the experimental tests, and were subjected to an acceleration time-history at their base [2]. A top mass was included to mimic the presence of the floors in a real building. Additionally, a non-linear interface at the bottom was used to consider the interaction with the surrounding soil [7].

Preliminary wall pre-damage investigations. In parallel, damage reports from houses exhibiting settlement damage were studied to determine typical crack patterns on various wall geometries. These were also incorporated into the wall

experiments by leaving plastic strips in the mortar joints [15]. The same crack patterns were replicated with the calibrated wall models and further compared against the experimental behaviour after in-plane loading.

Wall extrapolations with pre-damage and vibrations. Finally, the extrapolated models were used to analyse the effect of settlement pre-damage on the aggravation of vibration induced damage. Variations on the walls' material, soil properties, etc. were used to estimate the probability of crack-based light damage [2]. The proxy walls however, with single-wythe masonry and small geometries, were not representative of the geometry of historical façades; this limitation was reserved until additional insight could be gained about the geometry and settlement damage of historical geometries.

Study into bed-joint deformation and building damage. A thorough look into reports with measurements of bed-joint levels aimed to determine typical deformed shapes of masonry buildings subjected to settlements and relate them to the intensity of the observable damage. These shapes were further explored for more complex façade geometries and foundation types. It was determined that unreinforced foundations and long façades (with a length/height ratio larger than 1) were the most vulnerable to display damage when subjected to soil distortions [4, 5, 8].

2.2 Approach

In a similar manner as previous studies, the historical façades are first subjected to soil distortions causing a loss of support while being allowed to deform. Two variations of a façade are selected with a slightly different length/height ratio; see Figure 2. The façades sport tall windows on the ground floor and small openings on the first storey. Furthermore, they rest on a masonry wall enlargement, a typical masonry strip foundation herein simplified as a rectangular footing.

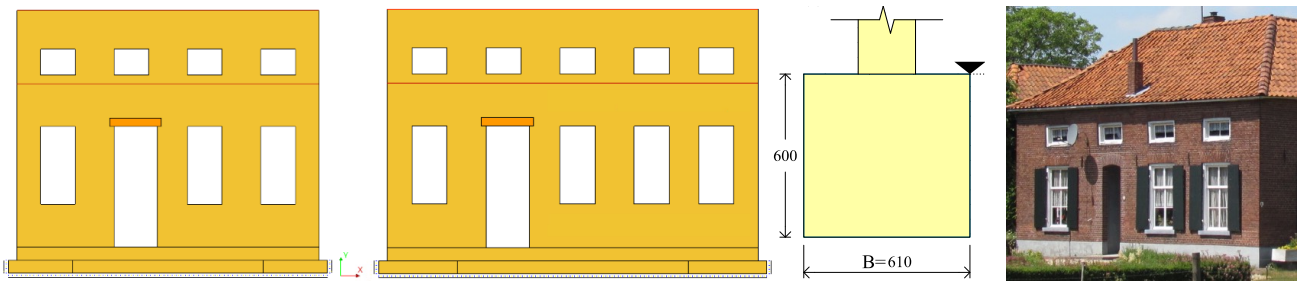

Fig. 2. Two selected geometries of an historical façade and its unreinforced masonry foundation. Photo on the right: typical farmhouse façade with small windows on the second storey; example from monument [16].

The finite-element-method models are plane-stress with a thickness of 0.2m for the walls, and 0.6m for the foundations. A rectangular mesh size of 0.1m is employed for both. The lintel of the door is of the same masonry material but with rotated local axis simulating the presence of a soldier pattern. Table 1 lists the selected masonry properties input for the non-linear material model. Additionally, a non-linear interface, depicted with a dotted line in Figure 2 and detailed in Table 2, is included in the model to represent the soil-foundation interaction. The interface employs a Coulomb Friction model with no cohesion and no tension with a friction angle of 30 and 20 degrees for sandy and peaty soil, respectively; the settlement shape is applied on the boundary end of the interface. The aim is to allow the building to deform naturally when subjected to the shape of the applied settlement, which corresponds to a loss of support, and not to enforce a particular shape since the deformation of the building in response to the reduced support cannot be known a-priori. Therefore, the interface includes the stiffness and damping of the surrounding soil for both vertical and horizontal directions; the definition of its parameters is done according to NERHP [11] and Longo et al. [7]. However, the horizontal direction is not active until sliding at the interface is locked during the time-history stage. In fact, the analyses include three phases: a first phase where the gravity loads are applied; a second phase where the settlement shape is enforced to the bottom side of the interface, and a last phase, where the time-history signal is introduced with a timestep of 1 ms. The line mass and corresponding loads at the roof and first floor levels are 225 and 100 kg/m respectively. Both façades have an opening ratio of 23% and a height of 5.5m, though the short façade is 7m long (L/H=1.27) while the long façade is 8.5m (L/H=1.54). Damping of 2%, in the form of Rayleigh damping, is employed based on the first two modes by participating mass.

Table 1. Masonry properties for the material model.

Material Properties	Symbol	Unit	Clay Masonry		
			Weak	Average	Strong
Density		kg/m^3		1950	
Elastic Modulus Perpendicular to Bed-Joints		MPa	3846	5000	7143
Elastic Modulus Parallel to Bed-Joints		MPa	1923	2500	3571
Elastic Shear Modulus		MPa	1538	2000	2857
Bed-Joint Tensile Strength		MPa	0.07	0.10	0.13
Minimum Head-Joint Tensile Strength		MPa	0.105	0.15	0.195
Tensile Fracture Energy		N/m	4.9	10	16.9
Vertical/Horizontal Compressive Strength		MPa	5.95	8.5	11.05
Vertical/Horizontal Compressive Fracture Energy		N/m	17431	18395	19312
Friction Angle (Friction Coefficient)		rad	0.448	0.64	0.832
Cohesion		MPa	0.105	0.15	0.195
Shear Fracture Energy		N/m	12.6	25.6	43.1
Crack band				Govindje	
Unloading in compression				Secant	
Head Joint Failure Option				Friction Based	
Predefined Angle for Diagonal Cracking		rad		0.50	

Table 2. Interface properties for the two soil profiles contrasted.
*Average values as the stiffness and geometry of the façades also affect these parameters.

Interface Properties			Soil Profile	
			Sandy	Peaty
Density	ρ	kg/m^3	1700	2000
Elastic Modulus	E	MPa	93.7	26.0
Elastic Shear Modulus	G	MPa	36.0	10.0
Poisson's Ratio	ν	-	0.3	0.3
Compression Wave Velocity	v_c	m/s	187.1	132.3
Shear Wave Velocity	v_s	m/s	100.0	70.7
Horizontal side stiffness*	kxsi	N/m^3	3.0E+08	8.4E+07
Horizontal side damping*	cxsi	N/m/s	2.2E+06	8.4E+05
Horizontal stiffness*	kxi	N/m^3	6.7E+07	1.9E+07
Horizontal damping*	cxi	N/m/s	6.5E+06	2.5E+06
Vertical stiffness*	kzi	N/m^3	9.5E+07	2.6E+07
Vertical damping*	czi	N/m/s	7.1E+06	2.8E+06
Vertical stiffness at corners*	kzei	N/m^3	4.0E+08	1.1E+08
Vertical damping at corners*	czei	N/m/s	3.2E+06	1.2E+06

Three settlement shapes are applied as depicted in Figure 3. An asymmetric hogging where only the left side of the façades lose support, a symmetric hogging where both sides lose support, and a symmetric sagging for which the centres of the façades become unsupported. The angular distortion of the shapes [19] is increased slowly in the models until a predefined intensity of damage appears with cracks in the order of 0.1 mm in width achieving a value of 1 for the Ψ damage parameter [12]. These narrow but visible cracks are later aggravated by the subsequent vibrations. Only cracks within light or serviceability damage are contemplated.

Six vibration signals are investigated. The signals have different properties so as to evaluate which type is more damaging. Four of the signals correspond to earthquake records and two belong to traffic. The latter were recorded at the top of the foundation of a building located a few metres from a road during the passing of a truck [9]. In another instance, a speedbump was present resulting in a time series with a frequency content with longer periods, as illustrated by the pseudo acceleration graph in Figure 3. For the M=3.4 earthquake of Zeerijp of 2018, two recordings from different stations are utilised, similarly for the M=3.4 earthquake of Westerwijtwerd of 2019. In both cases, a station close to the epicentre is contrasted to a station farther away. The "far" records have a greater number of effective cycles, longer periods, and greater significant duration [2]; in comparison, the "near" records display the characteristic "pulse" of induced events.

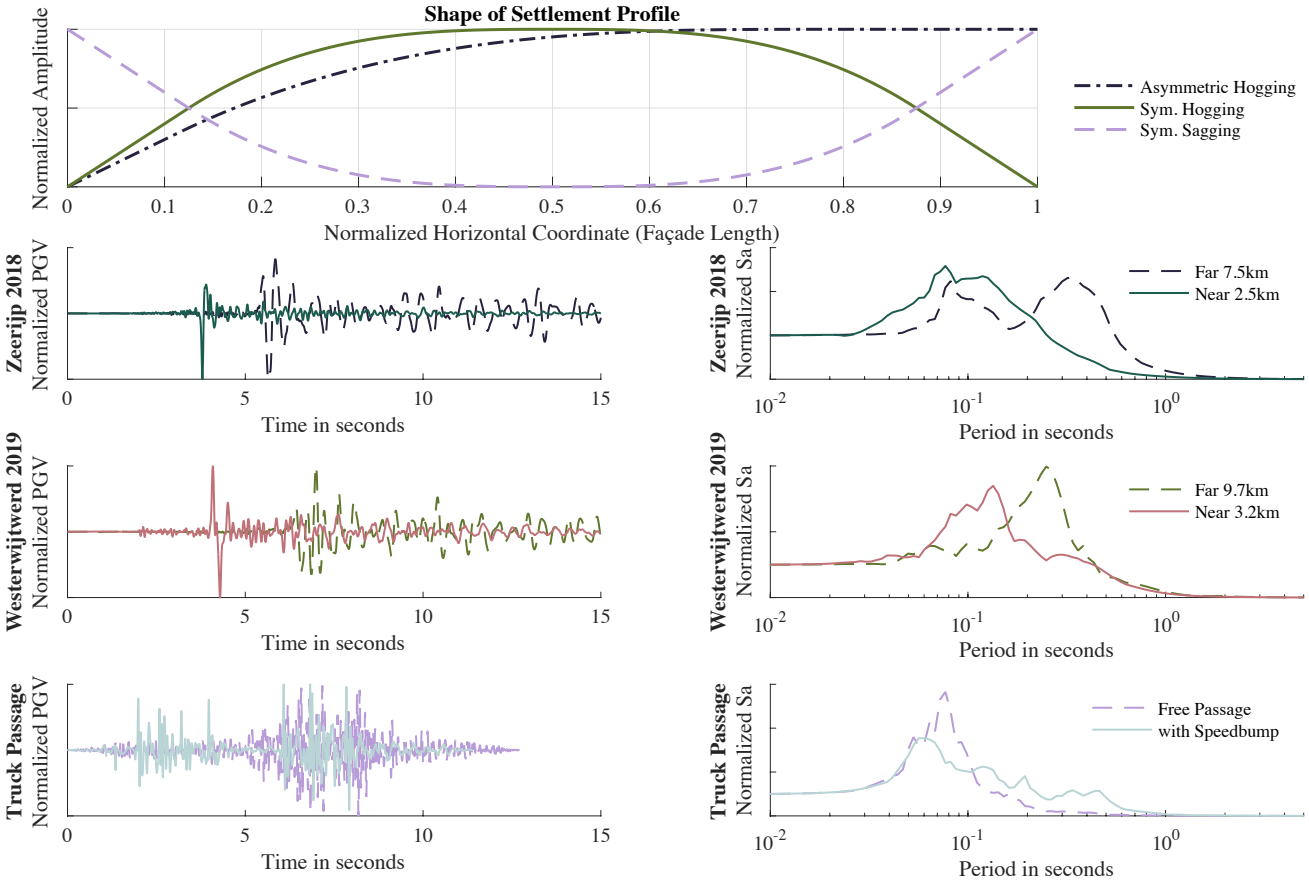

Fig. 3. Normalised settlement shapes considered, top; and normalised MaxRot horizontal component of the time-series employed in this paper for two earthquakes and the passage of a truck.

Damage was assessed using Ψ [12], an analytical parameter that compresses the damage pattern into a single number so that the initiation but mostly the aggravation of damage can be objectively measured and tracked among many models with different crack patterns in the plane of bare masonry walls. The parameter is computed from the number of cracks, and their width and length. With this approach, other parameters, such as the two façades mentioned, the three settlement shapes depicted, and the six vibration signals presented, were varied to evaluate their effect upon the initial and the increase in damage. Moreover, three additional parameters were varied: the material strength, contemplating a weaker and a stronger material; the initial damage, with no damage and Ψ_0=1; and, the Peak Ground Velocity of the signals. For the latter, the records presented in Figure 3 were amplified so that the horizontal PGV reached values of 2, 4, 8, 16, 32, and 64 mm/s. In comparison, the actual value measured at the near station of the record of Zeerijp reached about 31 mm/s. In total, 1728 model variations were analysed for this paper, comprising: 2 façades, 3 materials, 2 soil interfaces, 1 undamaged initial condition and 3 pre-damage settlement shapes, 6 vibration types and 6 vibration intensities.

3 Results

The models detailed in the previous section were analysed using DIANA FEA and the output of principal crack width (Ecw1 and Ecw3) was analysed automatically to characterise the cracks and determine the value of Ψ. A first subsection presents the results and the required soil distortion to cause a given intensity of pre-damage; while a more extended second subsection investigates the effect of vibrations on the (damaged) façades.

3.1 Applied soil distortion and damage

The flexible loss of support causes gravity to deform the façades which become damaged with small cracks. For this stage, a specific value of pre-damage was sought and thus a corresponding loss of support was determined. Figure 4 shows how cracks focused at the corner of the windows and reached barely-visible crack widths of 0.1mm, as per the definition for Ψ=1. The applied soil distortion, and its shape, is also visible in Figure 4, where it can be recognised how the façades, stiffer than the surrounding soil, do not cave in entirely at the locations where the loss of support is the greatest: at the corners, for the example of asymmetric hogging visible in Figure 4. Prosperi et.al. [5] determined that, as the façades become damaged, they also become more flexible and thus follow the soil distortion more closely. At Ψ=1, however, the distortion measured at the façades is much smaller than the applied distortion underneath the foundation. Figure 5 presents this comparison for the three settlement shapes investigated. The rightmost plot shows that lower values of distortion are required to reach the same damage intensity as with the other two shapes. In general, on the softer soils, a larger distortion is required; this makes sense since the softer interface is able to accommodate the imposed deformation and less of it is transferred to the façades. Similarly, the façades with weaker masonry material can also withstand larger applied deformations but also become damaged at lower measurable distortions on the walls; the stronger materials will require the largest distortions at Ψ=1. Finally, the longer façades seem to more easily follow the applied soil distortions and thus become damaged at lower distortions.

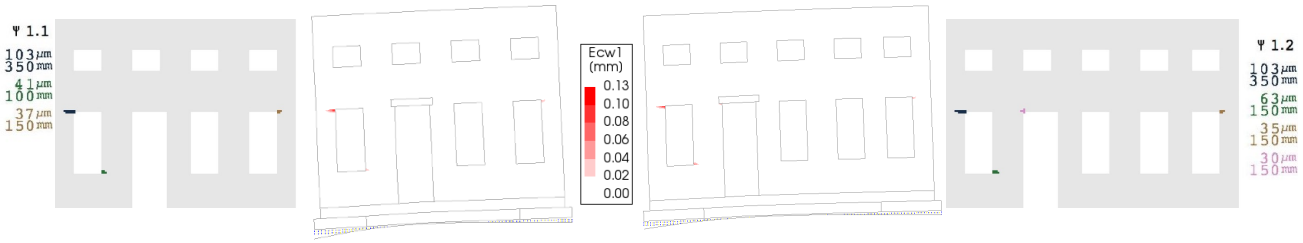

Fig. 4. Crack width (Ecw1) from the FEM model, center, for the short and long façades (left and right); and extremes, the automatically-processed damage value Ψ with interpreted crack pattern.

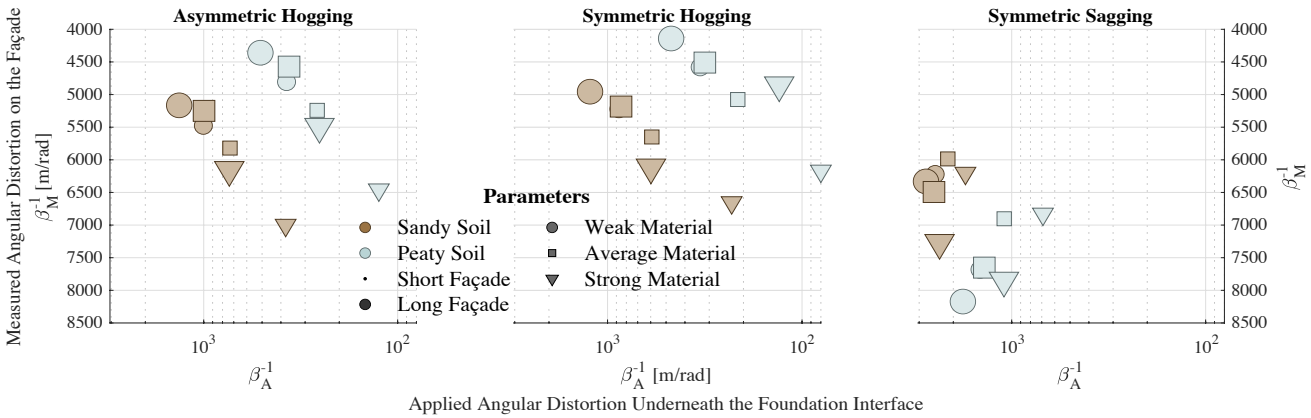

Fig. 5. Influence of the settlement shape (three graphs), the soil profile (marker colour), the façade length (marker size), and the relative material strength of the masonry (marker shape) on the required angular distortion applied (horizontal axis) to generate a pre-damage value of approx. Ψ=1 and the corresponding angular distortion measured on the façade (vertical axis). Distortions are inversed, e.g. 1/5000, 1/1000, etc. so top-right corners are most severe.

3.2 Vibrations and damage

The façade models, with and without initial damage as shown in section 3.1, were subjected to a vibration signal and evaluated with a non-linear, time-history analysis. In most cases, the vibrations caused new damage or aggravated the existing damage. Such is the case presented in Fig. 6, where the façades illustrated in Fig. 4 were subjected to the near signal of Zeerijp amplified to 32 mm/s. The earthquake doubled the damage intensity to Ψ=2 resulting in wider, longer, and additional cracks. In most cases, the existing cracks at the corners of windows were aggravated.

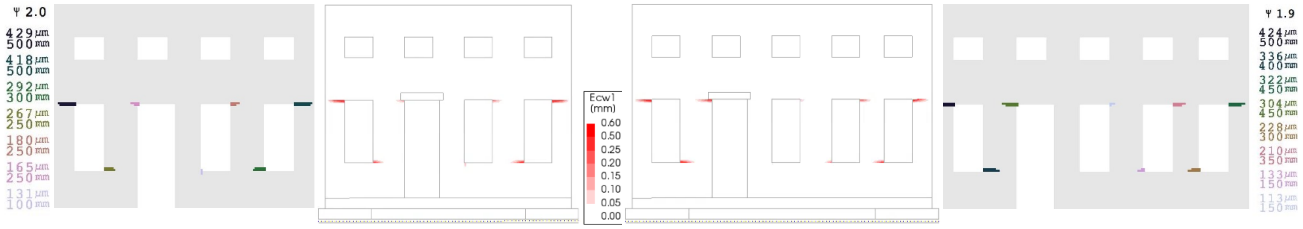

Fig. 6. Crack width from the FEM model, center, for the short and long façades (left and right); and extremes, the automatically-processed damage value. Situation after earthquake motion for pre-damaged example showcased in Fig. 4: existing cracks become aggravated and the damage increase (ΔΨ) is 0.9 and 0.7, respectively.

The results of the 1728 models run are gathered in Fig 7 and segregated by vibration type (earthquake or traffic) and PGV. As expected, higher PGV values lead to significantly more damage. Depending on the other parameters (material, soil, façade length, etc.) a varying damage increase is expected; the mean is pointed by the graph. It follows, that traffic vibrations are more damaging than earthquake vibrations when amplified to the same PGV; of course, it is unlikely that traffic vibrations will ever reach 64 mm/s, but the effect is hereby illustrated. At 2 mm/s, truck-induced vibrations lead to a damage increase of up to 0.5, while seismic vibrations only to about 0.2. However, earthquake vibrations lead to larger number of outliers deviating from the mean results, while the truck vibrations produce more uniform damage among the model pool. This is also observed in Fig 8 where the effect of all parameters is contrasted: the truck signals lead, on average, to a larger damage increase. In particular, the far earthquake records are less damaging to these two façades, followed by the truck record with a speedbump, the near earthquake records, and lastly, the free truck passage. Again, all amplified to identical PGV, while in reality the speedbump is likely to lead to larger PGV than the free passage of a truck. This is likely caused by the frequency content of the signals where higher frequencies affect the planar, stiff masonry façades the most. It is remarkable, however, that for the cases with initial pre-damage, the truck passages always lead to increased damage, while when no pre-damage is present, low PGV values also do not initiate damage.

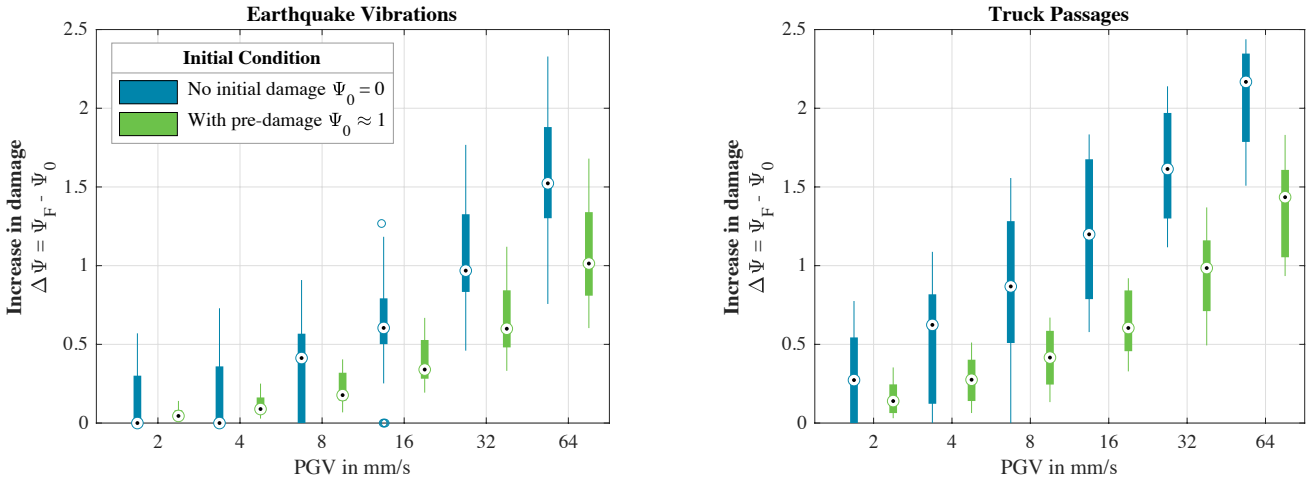

Fig. 7. Damage increase due to vibrations caused by earthquakes, left, and truck passages, right. The results of all model variations are pooled together with a mean indicated by the dotted circles, a 2nd-3rd quartile range shown by the boxes, and outliers shown outside the lines (≈ 2x standard deviation). Each PGV is further contrasted in terms of initial damage.

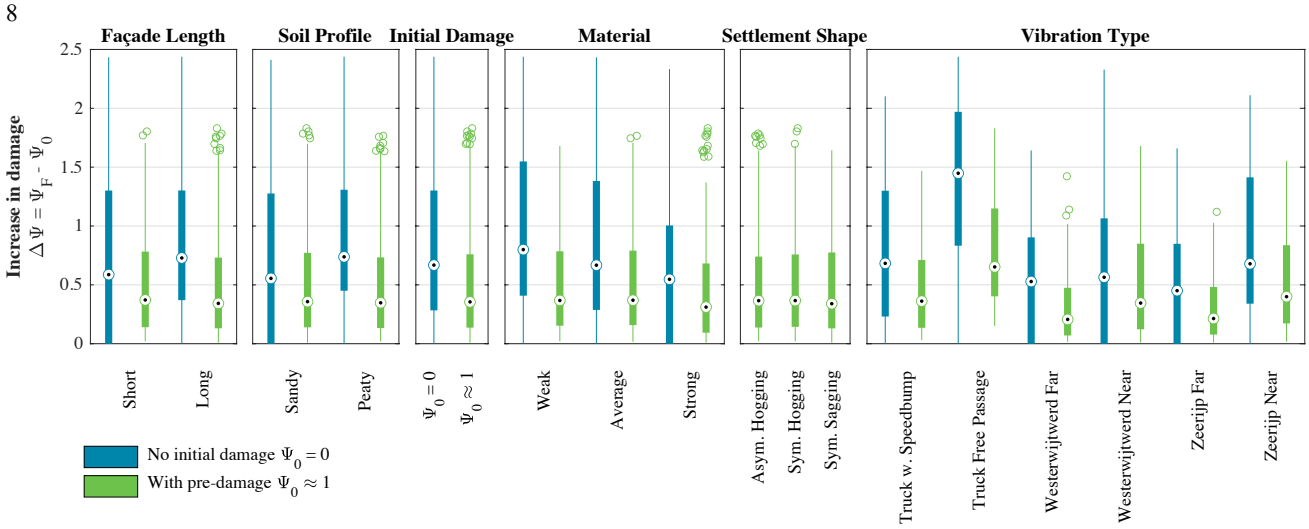

Fig. 8. Comparison of pooled results segregated only by the indicated parameters and, where applicable, the initial damage.

In contrast, the façade length and soil profile did not lead to large damage differences between the cases; however, the shorter façade and the sandy soil, when no initial damage had been applied, displayed less damage by the vibrations. The damage increase of the pre-damaged cases is lower than that of the virgin cases, except for very low PGVs when undamaged cases remain undamaged after the motion; this is recurrent in all the categories and summarised in the third box. However, the final damage of the pre-damaged façade is larger. It seems that pre-damage made the façades more flexible which allowed them to withstand the vibrations better; moreover, the existing damage already occupied the vulnerable spots in the façades and thus there were fewer locations for additional damage to develop. The stronger façades showed slightly less damage than the weak and average material masonry which is expected; however, this difference is less marked when the façades had sustained prior settlement damage. This is coherent with the hypothesis of damage making the façades more tolerant to additional damage. Finally, the shape of the applied soil distortion that caused pre-damage seems slightly influential when looking at the latter damage aggravation by the vibrations. For sagging shapes, a larger variation is observed, while asymmetric hogging displays the most outliers.

4 Discussion

As understanding of light, serviceability damage in masonry for settlement and vibration effects progresses, more complex models can be conducted. The study presented herein is such a step, where non-linear models of masonry walls are replaced by models of historical façades. Still, the new models are again a simplification of reality, focusing on 2D façades and in-plane effects with a limited number of façade geometries. Similarly, the interaction of the soil around the foundation is included for both settlement and time-history model phases, but follows from a simplification of the real foundation geometry and elastic properties for the soil behaviour. Nonetheless, the approach followed herein identified trends while being able to quantify and differentiate the effect of various parameters. Two parameters require further study. First, a distinction was observed between the applied soil distortion and the measured distortion on the façade. Fig 9, left, illustrates how the former is much larger than the latter and also shows a larger spread. While the reasons for this behaviour are understood (the applied distortion depends on more parameters and the measured distortion is more a property of the façade), how soil movements are transferred to foundations exactly, especially when horizontal strains are involved, needs to be investigated further. Secondly, in-plane thresholds are usually established by damage states linked to the drift of the buildings [10]. Fig 9, right, displays the relationship between drift and light damage as measured by Ψ. A trend can be recognised, but it can also be seen that, especially for values of Ψ around 2.5 (corresponding to the end of light damage), a large interval of drift is associated with damage. This graph also shows how a PGV value of 2 or 4 mm/s can generate drift without in-plane damage, or vice-versa where no drift is observed but visible damage appears. Moreover, the graph shows that towards the end of light damage, the influence of the initial condition on the final damage diminishes.

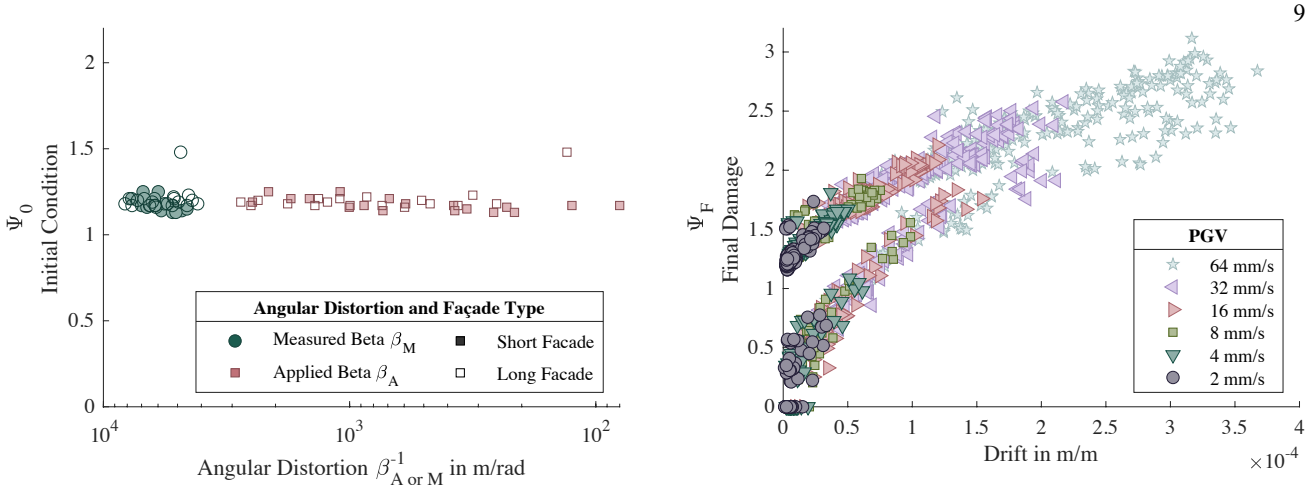

Fig. 9. Relationship between the angular soil distortion and damage, left; and right, between horizontal in-plane drift and damage.

An important comparison can be made against the proxy walls of the initial study [2]. Fig 10 shows that the historical façades appear significantly more vulnerable to earthquake vibrations. This is not entirely unexpected since the material properties for the historical masonry are more sensitive. However, for small values of PGV, the walls remain mostly undamaged, while the façades do become damaged; this may be attributable to the more complex geometry, heavier double-wythe walls, and larger opening ratios of the historical façades. The comparison is performed only for earthquake vibrations, as the walls were not evaluated with traffic vibrations; but, since the truck vibrations have shown to be more detrimental, the vulnerability of the historical façades against traffic vibrations should not be underestimated.

The case-based study looking at the potential causes of damage conducted in 2018 [3], concluded that the likelihood of visible damage being attributable to earthquake vibrations around 2 mm/s, was unimportant. This is in line with our observations, since Ψ and $\Delta\Psi$ values remain very well below the visible thresholds of 1 and 0.5 respectively.

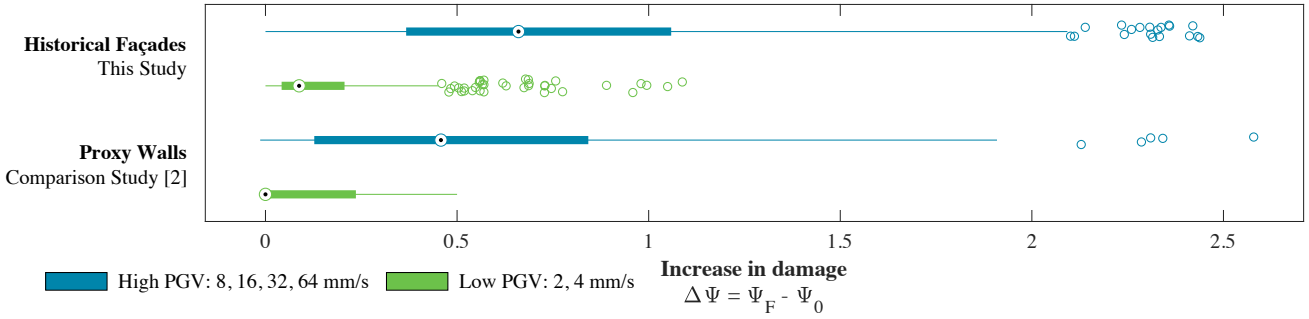

Fig. 10. Comparison between walls and historical façades only for earthquake vibrations. An increase in damage of 0.5 is visible to the naked eye. The range of parameters has been restricted for the walls so as to generate a one-to-one comparison.

5 Conclusions

This modelling study has assessed two geometrical variations of a double-wythe, fired-clay brick masonry façade subjected to varying settlement shapes and subsequently, to seismic and traffic vibrations. The goal is to establish a relationship between these processes, several façade properties, such as their length and material strength, and the development of light, crack-based damage on the façades. We have observed that:

- At low values of damage, only a small amount of the soil distortion underneath the façade foundations is transferred to the masonry leading to cracks.
- Longer façades required a smaller applied soil distortion to develop visible damage in comparison to shorter façades. Similarly, these façade geometries were more vulnerable to sagging settlement shapes than hogging shapes. The settlement shape did not affect the damage increase caused by subsequent vibrations.

- Vibrations, even with low PGV values of 2 mm/s, increased visible damage in most cases, while seldom initiated cracks in undamaged façades. In particular, traffic vibrations lead to increased damage in all pre-damaged cases investigated.
- At low values of PGV, traffic vibrations lead to twice as much damage as earthquake vibrations, and to about 30% more damage at high values of PGV; though these high PGVs are not expected for traffic vibrations.
- Horizontal drift values of 0.4‰ are associated with the upper boundary of light damage for these historical façades; much lower than comparable drift limits established for DS1 of regular masonry buildings.
- In fact, when compared against simple masonry walls from an earlier study [2], seismic vibrations were about 40% more damaging to the historical façades, and even more severe in the range of 2-4 mm/s.

These observations warrant future, more in-depth analyses looking at important effects such as the transfer of soil deformations to the shallow foundations, typical of historical heritage, 3D building effects so far neglected, so as interlocking with transversal walls, the participation of the floors and their potential restraining effect, additional vibration sources and more measurements of traffic vibrations on actual buildings, and more complex structural typologies and variations.

References

1. P.A. Korswagen, M. Longo, E. Meulman, J.G. Rots (2019). Crack initiation and propagation in unreinforced masonry specimens subjected to repeated in-plane loading during light damage. Bull Earthquake Eng. 17. doi.org/10.1007/s10518-018-00553-5
2. P.A. Korswagen, M. Longo, J.G. Rots (2022). Fragility curves for light damage of clay masonry walls subjected to seismic vibrations. Bull Earthquake Eng doi.org/10.1007/s10518-022-01404-0
3. P.C. Van Staalduinen, K. Terwel, J.G. Rots (2018). Onderzoek naar de oorzaken van bouwkundige schade in Groningen Methodologie en case studies ter duiding van de oorzaken.TU Delft. Report CM-2018-01, 11 July 2018.
4. A. Prosperi, P.A. Korswagen, M. Korff, R. Schipper, J.G. Rots (2023). Empirical vulnerability and fragility curves for masonry buildings subjected to settlements. Journal of Building Engineering (UNDER REVIEW)
5. A. Prosperi, M. Longo, P.A. Korswagen, M. Korff, J.G. Rots (2023). Sensitivity modelling with objective damage assessment of unreinforced masonry façades undergoing different subsidence settlement patterns. Engineering Structures (UNDER REVIEW)
6. S. Jafari (2021). Material characterisation of existing masonry: A strategy to determine strength, stiffness and toughness properties for structural analysis. TU Delft doi.org/10.4233/uuid:3bcbbc72-0212-44e9-ac86-2fdc54ec5987
7. M. Longo, M. Sousamli, P.A. Korswagen, P.C. Van Staalduinen, J.G. Rots (2020). Three-tiered finite element approach to soil-masonry-wall interaction for light seismic motion. Eng Struct 245:2021. doi.org/10.1016/j.engstruct.2021.112847
8. P.A. Korswagen, M. Longo, J.G. Rots, A. Prosperi (2022). Supporting analyses to determine probability of damage and fragility curves due to indirect subsidence effects. Delft University of Technology. Final Version 2, October 3, 2022.
9. D. Moretti, A.J. Bronkhorst, C.P.W. Geurts (2020). Characterization of vibrations for the Groningen building monitoring network. TNO Report 2019 R11991
10. C. Del Gaudio, M.T. De Risi, P. Ricci, G.M. Verderame (2017). Drift-based fragility functions for hollow clay masonry infills in RC buildings under in-plane seismic actions. Anidis, 2017, Pistoia.
11. NEHRP (2012). Soil-Structure Interaction for Building Structures. NIST GCR 12-917-21 U.S. Department of Commerce National Institute of Standards and Technology.
12. P.A. Korswagen & J.G. Rots (2020). Monitoring and quantifying crack-based light damage in masonry walls with Digital Image Correlation. 1st International Conference on Structural Damage Modelling and Assessment (SDMA), Gent, Belgium 2020
13. A. Prosperi, M. Longo, P.A. Korswagen, M. Korff, J.G. Rots (2023). Accurate and efficient 2D modelling of historical masonry buildings subjected to settlements in comparison to 3D approaches. 13th SAHC, September 2023, Kyoto, Japan.
14. G.M.A. Schreppers, A. Garofano, F. Messali, J.G. Rots (2016). DIANA validation report for masonry modelling. DIANA FEA report 2016-DIANA-R1601 TU Delft Structural Mechanics Report CM-2016-17, 143 pp.
15. P. Korswagen, M. Longo, E. Meulman, J.G. Rots (2019). Experimental and Computational Study of the Influence of Pre-Damage Patterns in Unreinforced Masonry Crack Propagation Due to Induced, Repeated Earthquakes. 13th NAMC, July 2019 Utah, USA.
16. Monumental Farmhouse, National Monument ID: 523688. Retrieved January 2023. https://rijksmonumenten.nl/monument/523688/boerderij-met-aangrenzende-bijschuren/breedenbroek/
17. Peduto, D., Prosperi, A., Nicodemo, G., & Korff, M. (2022). District-scale numerical analysis of settlements related to groundwater lowering in variable soil conditions. *Canadian Geotechnical Journal*, *59*(6), 978-993.
18. Costa, A. L., Kok, S., & Korff, M. (2020). Systematic assessment of damage to buildings due to groundwater lowering-induced subsidence: Methodology for large scale application in the Netherlands. *Proc. Intl. Assoc. Hydrological Sciences*, *382*, 577-582.
19. J.B. Burland, C.P. Wroth (1974). Settlement of buildings and associated damage. Proceedings of Conference on Settlement of Structures, pages 611–654, Cambridge, 1974. Pentech Press.